12th International Symposium on Turbulence and Shear Flow Phenomena (TSFP12)
Osaka, Japan (Online), July 19-22, 2022

RESPONSE OF HIGH REYNOLDS NUMBER TURBULENT PIPE FLOW TO THE PRESENCE OF AN AXISYMMETRIC BODY

Ian E. Gunady
Department of Mechanical and Aerospace Engineering
Princeton University
Princeton, NJ 08544
igunady@princeton.edu

Liuyang Ding
Department of Mechanical and Aerospace Engineering
Princeton University
Princeton, NJ 08544
liuyangd@princeton.edu

Marcus Hultmark
Department of Mechanical and Aerospace Engineering
Princeton University
Princeton, NJ 08544
hultmark@princeton.edu

Alexander J. Smits
Department of Mechanical and Aerospace Engineering
Princeton University
Princeton, NJ 08544
asmits@princeton.edu

ABSTRACT

Effects from pressure gradients, streamline convergence/divergence, and streamline curvature are often encountered in engineering wall-bounded flows. For example, as the flow passes over a fuselage or hull, it encounters a favorable pressure gradient and streamline curvature and divergence as it is accelerated past the nose. The flow then relaxes over the midbody of the vehicle before encountering an adverse pressure gradient and streamline curvature and convergence over the stern. Past the vehicle, the flow forms a wake that subsequently decays.

Scaling laws and modeling approaches developed for canonical wall-bounded turbulence may require modifications when such non-equilibrium conditions are present. Previous studies that have explored the effects of pressure gradients and surface curvature have typically studied these effects separately. For example, Harun *et al.* (2013) showed that an adverse pressure gradient energizes turbulence while a favorable pressure gradient suppresses turbulence. Similarly, Smits *et al.* (1979); Muck *et al.* (1985) and Hoffmann *et al.* (1985) noted that convex surface curvature has a stabilizing effect on turbulent boundary layers while concave surface curvature has a destabilizing effect. Also, Nagib & Chauhan (2008) found that the slope of the log law region may be affected by pressure gradient and flow geometry. After strong perturbations such as a change in roughness, a short region of surface curvature, or a short region of separated flow, a non-monotonic second order recovery is often observed where the initial recovery of the $\overline{u_s^2}$ profile overshoots the equilibrium profile (Smits *et al.*, 1979; Ding *et al.*, 2021). Experiments on the effects of simultaneous perturbations, such as streamline curvature and divergence with pressure gradient, are very rare, and most of the existing experiments on strong perturbations have been conducted at only moderate Reynolds numbers, so the effects of high Reynolds numbers relevant for many engineering applications are also largely unknown.

In this work, an axisymmetric body of revolution (BOR) is placed at the centerline of the Superpipe facility at Princeton University. The flow far upstream and downstream of the BOR is high Reynolds number, fully developed turbulent pipe flow, and the evolution of turbulence through the different conditions encountered around the body of revolution is explored. This work furthers our understanding of wall-bounded turbulence in complex flows, and provides a challenging test case for turbulence models (Visonneau *et al.*, 2022).

EXPERIMENTAL SETUP

Experiments are conducted in the Superpipe facility modified to accommodate the axisymmetric body. The pipe has an inner diameter $D = 2R = 129$ mm and a development length of $200D$ upstream of the first measurement location. Further details of the facility are given by Zagarola & Smits (1998). The Reynolds numbers Re_D based on pipe diameter and bulk velocity of the incoming fully developed turbulent pipe flow are varied between 0.2×10^6 and 5×10^6, corresponding to $Re^+ = Ru_\tau/\nu$ between $4,500$ and $80,000$, where $u_\tau = \sqrt{\tau_w/\rho}$, τ_w is the wall shear stress, ρ is the density, and ν is the kinematic viscosity.

The geometry of the axisymmetric body follows closely the geometry of a similar experiment described by Ding *et al.* (2019) and Saxton-Fox *et al.* (2019) in a water pipe at a lower Reynolds number. The body is held at the centerline of the Superpipe by a 2D airfoil-shaped sting. The area blockage ratio of the body in this work is $\gamma = d^2/D^2 = 2/9$ and future experiments will also include $\gamma = 1/9$ and $1/3$. The body is composed of three parts: the bow, midbody, and stern. Figure 2 shows an outline of the BOR profile with vertical lines separating the bow, midbody, and stern. The bow's profile is a prolate spheroid with length $l_b = 4D/3$ satisfying

$$\frac{x^2}{l_b^2} + \frac{y^2}{(d/2)^2} = 1 \tag{1}$$

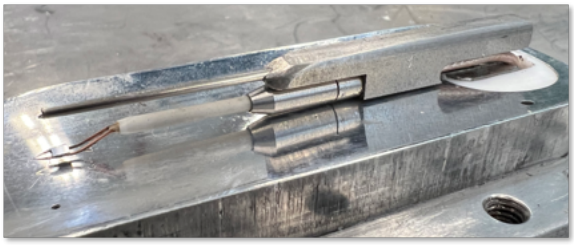

Figure 1: A low-profile sting holding the NSTAP and pitot probe.

where $x \in [-l_b, 0]$ and d is the diameter of the center body. The midbody is a straight cylindrical section with length $5D/3$, and the stern section has a length $l_s = 4D/3$ and follows a power function satisfying

$$y = \pm\frac{d}{2}(1 - \frac{x^4}{l_s^4}) \tag{2}$$

where $x \in [0, l_s]$.

Data are taken using a nanoscale thermal anemometry probe (NSTAP) (Bailey *et al.*, 2010; Vallikivi *et al.*, 2011; Vallikivi & Smits, 2014) mounted on a probe holder that traverses in the radial direction. A low profile probe holder shown in figure 1 was used to minimize blockage. The geometry of the probe holder allowed measurements close to the surface of the pipe, but limited access to locations close to the BOR surface. The probe was fixed at a given streamwise location, and to gain access to various streamwise locations the sting holding the BOR was fixed to a carriage and rail mounted on the pipe wall. A linear drive system placed $16D$ downstream of the measurement probe allowed the BOR to move $14D$ in the streamwise direction relative to the fixed probe. The rail and carriage system occupied 0.6% of the pipe cross section so that its blockage effects were negligible, and the measurement probe was located diametrically opposite the rail system.

RESULTS

Data were taken on an axial-radial plane intersecting the axis of the pipe between $x/R = -1.5$ and 12.5 (about $4R$ downstream of the stern), where $x/R = 0$ is located at the nose of the BOR and R is the pipe radius. The wall-normal direction is denoted by y/R where $y/R = 0$ is the pipe wall. For the data presented here, the Superpipe facility was operated at a bulk velocity $U_b = 10.4$ m/s, Reynolds number based on pipe diameter $Re_D = 490,000$, friction Reynolds number $Re^+ = 10,000$, and upstream friction velocity $u_\tau = 0.43$ m/s. Figure 2 shows points where data are taken as well as the BOR profile and pipe wall. These data are collected using a NSTAP with non dimensional length $l^+ = l/l_\nu = 9.4$ where l_ν is the viscous length scale based on the upstream friction velocity.

Upstream and Bow

The mean flow at various streamwise locations upstream of the BOR and in the region of the bow are shown in figure 3. The wall-normal coordinate y is normalized by Y_t which is equal to the pipe radius R upstream and downstream of the BOR, and elsewhere equal to the distance between the pipe wall and the surface of the BOR. The mean velocity is shown normalized by the upstream bulk velocity (figure 3a) as well as the local bulk velocity $U_{bx} = U_b R^2/(Y_t(2R - Y_t))$ (figure 3b). Reynolds normal stress profiles normalized by upstream friction velocity u_τ are shown in figure 4.

The mean flow and Reynolds normal stress profiles at $x/R = -1.46$ and $x/R = -0.70$ are almost identical, suggesting that both these locations are far enough upstream to be unaffected by the presence of the BOR and accurately represent the upstream inflow conditions. Further downstream, the mean flow and turbulence profiles change as the presence of the BOR causes a bulk flow acceleration, while a boundary layer forms over the surface of the BOR. The mean flow profiles clearly show the acceleration of the flow over the bow section as the cross-sectional area decreases. The Reynolds normal stress profiles show that as the flow is accelerated over the nose, the turbulence in the bulk flow is initially suppressed, while the region near the surface of the pipe thins. The turbulence then grows as the flow enters the straight section. Away from the wall of the pipe, the Reynolds normal stress profiles shown in figure 4 agree well with PIV data collected by Ding *et al.* (2019) in a companion experiment in a water pipe at $Re^+ = 3,550$, despite the differences in Reynolds number. Close to the wall, however, the PIV data were significantly filtered by spatial resolution effects, whereas the current NSTAP data are not limited in this respect and so are more accurate. In contrast, the PIV data was able to resolve the flow close to the surface of the BOR, which was not possible using the current probe design.

The velocity spectra can help to examine how the energy content between various scales changes in various regions of the flow. Figure 5 shows pre-multiplied streamwise velocity spectra close to the pipe wall at $y/Y_t = 0.015$ and away from the pipe wall at $y/Y_t = 0.28$ and 0.51. We use the local bulk velocity U_{bx}, based on the upstream bulk velocity and the geometry of the BOR, as a measure of the local convective velocity. Also, a constant value y/Y_t is a rough approximation to following a streamline close to the wall. As already noted in figure 4, at $y/Y_t = 0.015$ we see an initial reduction in overall energy content followed by an increase at $x/R = 2.43$ as the flow enters the mid-body section. Further from the wall, at the $y/Y_t = 0.28$ or 0.51 locations, there is less turbulent energy and a general shift in the energy distribution towards larger scales compared to the near-wall location. In this scaling, the spectra at the larger scales (lower frequencies) collapse suggesting that the local bulk velocity and the spacing between the BOR and the pipe wall are the correct scales for the outer layer motions.

The differences in the spectra shown in figure 5 are also telling. Close to the wall, local bulk velocity is not the right scale for the energy content as seen by the lack of collapse in the middle region of the spectra. However, away from the wall there is some collapse for the $x/R = -1.45$ and 0.19 locations, suggesting that the energy content away from the wall may initially scale with local bulk velocity. This is opposed to the near-wall locations where there is no collapse of overall energy content. It is also important to note that some of the difference observed near the wall at various streamwise positions can be attributed y^+ changing due to the changing pressure gradient even as y/Y_t stays constant.

Straight Development Section

After the bow region of the BOR, the flow enters the straight cylindrical midbody region where bulk flow acceleration and streamline curvature no longer have an affect. Figure 6a shows growth of the low-momentum near-wall shear layer and acceleration of the flow in the middle of the annulus. Given enough development length, the mean flow profile

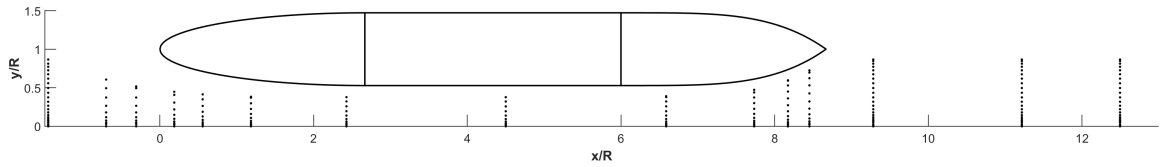

Figure 2: An axial-radial cross section of the BOR and pipe wall are shown. Points where data are taken are denoted by dots. x/R describes the streamwise location relative to the nose of the BOR and y/R denotes position relative to the pipe wall. Vertical lines on the BOR separate the bow, straight cylindrical, and stern sections of the BOR.

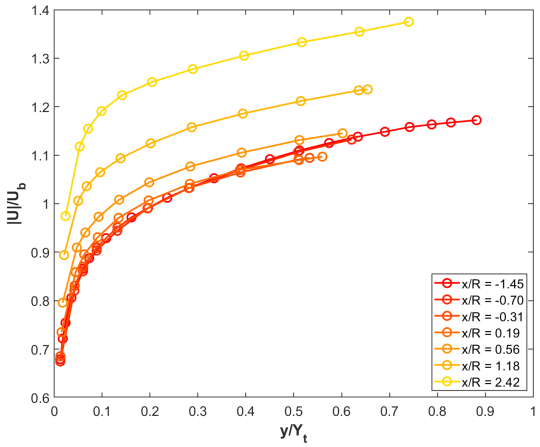

(a) Mean flow normalized by upstream bulk velocity U_b.

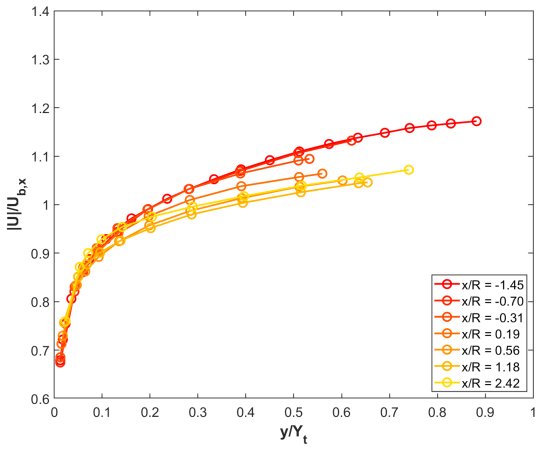

(b) Mean flow normalized by local bulk velocity $U_{b,x}$.

Figure 3: Mean flow upstream of the BOR and in the region of the bow.

would relax to fully developed annular flow profile. However, the flow encounters the stern section of the BOR well before this can happen.

Stern and Wake

Figure 6b shows mean flow profiles in the stern region of the BOR and in the wake. In the stern, there is a bulk deceleration of the flow as well as a pronounced velocity deficit around the centerline that grows in the stern region as seen in the profiles from $x/R = 6.59$ to $x/R = 8.45$. As the velocity deficit is growing, the shear layer near the pipe wall thickens due to the adverse pressure gradient and streamline divergence. Between $x/R = 9.28$ and $x/R = 12.49$ the velocity deficit begins to recover in the BOR's wake and the shear layer close to the pipe wall continues to thicken as the flow recovers towards fully developed pipe flow.

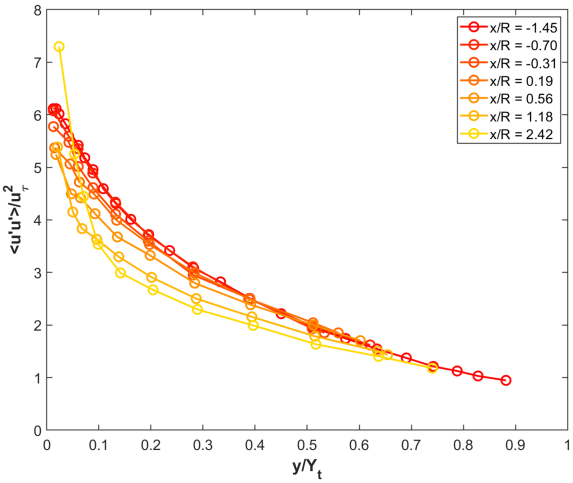

Figure 4: Reynolds normal stress upstream of the BOR and in the region of the bow.

CONCLUSIONS

NSTAP data are taken for a canonical axisymmetric geometry placed in the Princeton Superpipe facility. The geometry features favorable and adverse pressure gradients, streamline convergence and divergence, and streamline curvature. The body used in this work is composed of three sections: the bow, straight cylindrical section, and stern. As the flow accelerates past the bow section, turbulence is suppressed and the near-wall shear layer shrinks. Analysis of spectra suggest that in the bow region, the large turbulent scales with the local bulk velocity and spacing between the BOR and pipe wall. In the straight cylindrical section, the flow relaxes and the near-wall shear layer grows before encountering the stern where the shear layer grows again as the flow decelerates and expands. A pronounced velocity deficit grows in the stern region before recovering in the wake of the BOR. Results in this work align well with previous results obtained using PIV in a water pipe of a similar geometry (Ding *et al.*, 2019; Saxton-Fox *et al.*, 2019). This work provides data close to the pipe wall where PIV experiences near-wall filtering. Future analysis of these data includes a deeper look into Reynolds normal stress and spectra in the straight cylindrical section, the stern, and the wake of the BOR along with a more robust scaling for the mean velocity profiles and spectra. Future works will also traverse a range of Reynolds numbers and BOR blockage ratios.

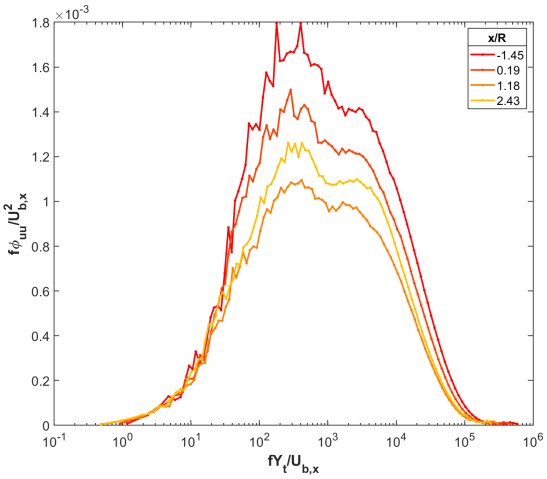

(a) $y/Y_t = 0.015$

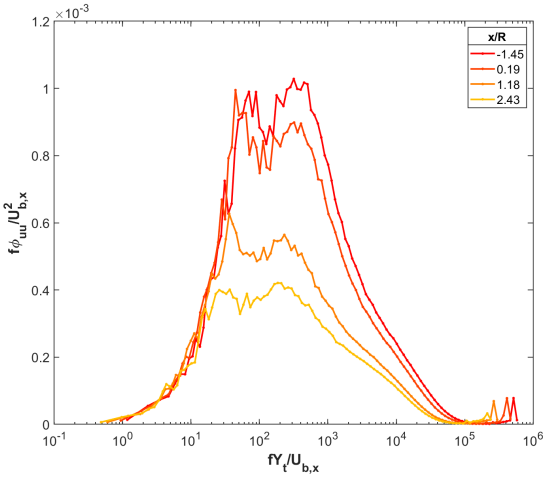

(b) $y/Y_t = 0.28$

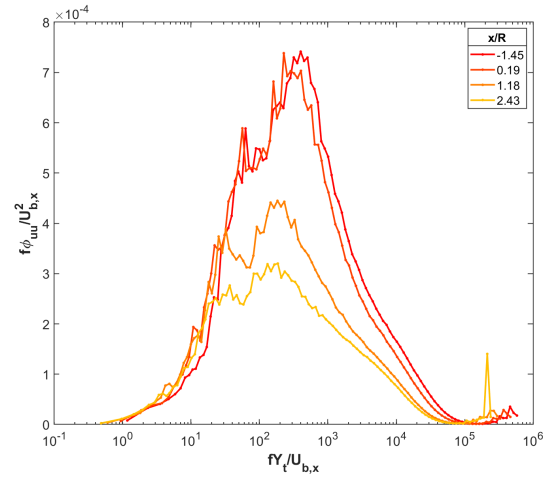

(c) $y/Y_t = 0.51$

Figure 5: Premultiplied streamwise velocity spectra at $x/R = -1.45, 0.19, 1.18, 2.43$.

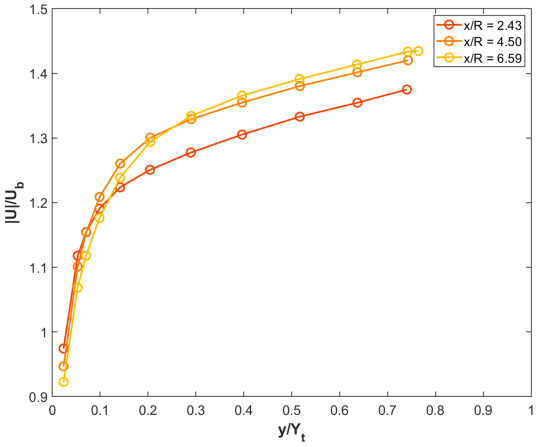

(a) Midbody

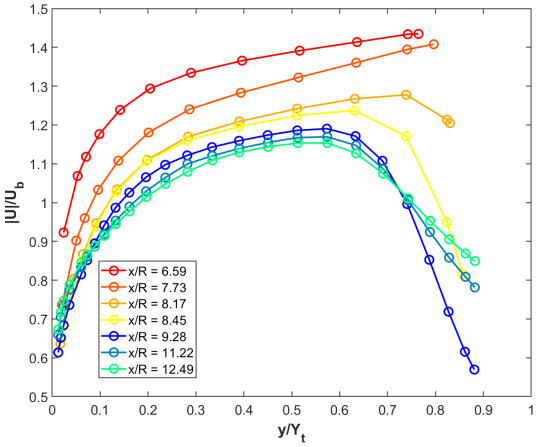

(b) Stern and wake

Figure 6: Mean flow normalized by upstream bulk velocity for the midbody, stern, and wake of the BOR.

ACKNOWLEDGEMENTS

I.E.G. was supported by the National Defense Science and Engineering (NDSEG) Fellowship Program. Additional support was received under ONR Grants N00014-17-1-2309 and N00014-19-1-2301 (Program Manager Peter Chang).

REFERENCES

Bailey, S. C. C., Kunkel, G. J., Hultmark, M., Vallikivi, M., Hill, J. P., Meyer, K. A., Tsay, C., Arnold, C. B. & Smits, A. J. 2010 Turbulence measurements using a nanoscale thermal anemometry probe. *J. Fluid Mech.* **663**, 160–179.

Ding, L., Saxton-Fox, T., Hultmark, M. & Smits, A. J. 2019 Effects of pressure gradients and streamline curvature on the statistics of a turbulent pipe flow. In *11th Inter. Symp. on Turbulence and Shear Flow Phenomena, TSFP 2019*.

Ding, L., Van Buren, T., Gunady, I. E. & Smits, A. J. 2021 Perspective on the response of turbulent pipe flows to strong perturbations. *Fluids* **6** (6), 208.

Harun, Z., Monty, J. P., Mathis, R. & Marusic, I. 2013 Pressure gradient effects on the large-scale structure of turbulent boundary layers. *J. Fluid Mech.* **715**, 477–498.

Hoffmann, P. H., Muck, K. C. & Bradshaw, P. 1985 The effect of concave surface curvature on turbulent boundary layers. *J. Fluid Mech.* **161**, 371–403.

Muck, K. C., Hoffmann, P. H. & Bradshaw, P. 1985 The effect of convex surface curvature on turbulent boundary layers. *J. Fluid Mech.* **161**, 347–369.

Nagib, H. M. & Chauhan, K. A. 2008 Variations of von kármán coefficient in canonical flows. *Phys. Fluids* **20** (10), 101518.

Saxton-Fox, T., Ding, L., Smits, A. J. & Hultmark, M. 2019 Coherent structure deformation in a turbulent pipe flow

with a spatially-developing pressure gradient. In *11th Inter. Symp. on Turbulence and Shear Flow Phenomena, TSFP 2019*.

Smits, A. J., Young, S. T. B. & Bradshaw, P. 1979 The effect of short regions of high surface curvature on turbulent boundary layers. *J. Fluid Mech.* **94** (2), 209–242.

Vallikivi, M., Hultmark, M., Bailey, S. C. C. & Smits, A. J. 2011 Turbulence measurements in pipe flow using a nano-scale thermal anemometry probe. *Exp. Fluids* **51**, 1521–1527.

Vallikivi, M. & Smits, A. J. 2014 Fabrication and characterization of a novel nano-scale thermal anemometry probe. *J. Microelectromechanical Systems* **23** (4), 899–907.

Visonneau, M., Guilmineau, E., Deng, G., Ding, L. & Smits, A. J. 2022 Bodies-of-revolution in turbulent flow: comparing computation with experiment. *AIAA Paper 2022-0694* .

Zagarola, M. V. & Smits, A. J. 1998 Mean-flow scaling of turbulent pipe flow. *J. Fluid Mech.* **373**, 33–79.